Atmospheric Modeling Around a City to Study the Effects of a Nearby Pollutant Source on Air Quality

Edward Guo (jguo4)
Joe Joseph (joej)
Pranshu Pant (ppant)

ABSTRACT

Growing population in urban environments has raised concern for the collective well-being of its residents, with air pollution being one of the major concerns. In our project, we have set out to model the ill effects of having pollution sources in the vicinity of a city. Power plants are a source of constant heat and pollution. While they are designed for maximum thermal efficiency and economy in mind, the long-term health impacts due to pollution should also be taken into account. A 2D transient incompressible Navier-Stokes solver was developed in Python that models energy and scalar transport, incorporating buoyancy effects. 2D CFD parametric studies were performed on vertical positions of pollutant source and building configurations. Our study establishes the need for computational analysis as a tool for policy decisions and regulations for city layouts and power plant locations. We have also augmented our solver to solve for turbulent flows in the form of large eddy simulation (LES).

INTRODUCTION AND BACKGROUND

The homes and businesses in large cities are sustained by a lot of energy, in the form of electricity, heat, and gas. This energy comes at an environmental cost. In the state of Pennsylvania, in Aug 2019, the Energy Information Administration [3] recorded 44,000 barrels of petroleum, and 1,730 short tons of coal used for electricity generation. Given an extraction efficiency of ~50%, a lot of waste gas, particulate matter and heat are emitted in burning all that fossil fuel. The waste gas and aerosols emitted in producing all this energy raise concern for nearby residents, especially if there are densely populated cities nearby to raise energy demand. As shown in Figure 1, most of the power plants congregate around big cities, such as Pittsburgh, and Philadelphia [2]. Specifically, coal combustion releases large amounts of particulate matter, sulfur dioxide and nitrogen dioxide, all of which contribute to smog and cultivate respiratory illnesses and lung diseases. When dissolved in rainwater, sulfur dioxide contributes to the formation of acid rain, causing harm to all organic matter that comes into contact. As of nuclear fission power plants using uranium, almost all the nuclear power plants in the U.S. were built more than 35 years ago [1]. Outdated technologies make these nuclear power plants vulnerable to nuclear meltdown, in which case toxic and radioactive chemicals would be released into the atmosphere unrestrained, causing genetic abnormality not only to people directly in contact, but also to people exposed to the radiation.

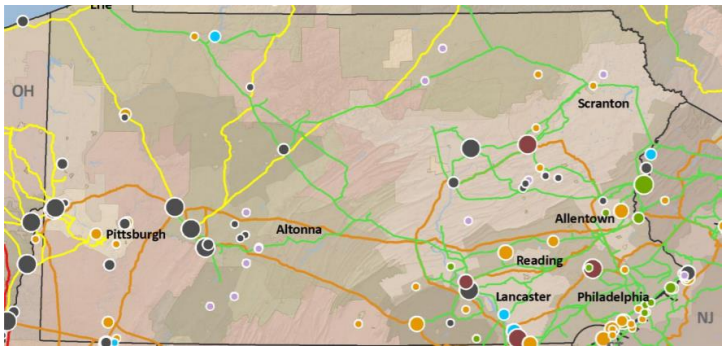

Figure 1. A map of Pennsylvania, showing major cities, and locations and sizes of power plants. The circles shades grey represents coal-fired power plants, orange represents natural gas and burgundy represents nuclear fission plants using uranium.

The project detailed in this report is aimed at addressing the concern for the city residents' health by building a 2-D atmospheric model, to simulate the transport of a generic pollutant and temperature emitted from a source outside the city. The numeric model that is built will solve the x and y-components of Navier-Stokes equations. Along the y-direction, buoyancy effect is considered by adding a Boussinesq approximation using temperature output from the energy equation. A scaled-up version of this model can be used to track the aerosol waste and heat emissions from factories near cities, given a wind speed. The model outputs the concentration of the pollutants and temperature distribution in the 2-D field, at an end time specified by the user.

PROBLEM SET-UP

Flow Assumptions:

- The flow is 2-D planar.
- The flow is in the laminar regime within the domain (Re_x << 5E+5). To keep Reynolds number, $Re_x = u\,x/\nu$ within threshold, the inlet velocity, domain size and the kinematic viscosity of air needs to be adjusted for this assumption to hold true. (NOTE: LES is also solved but is not used for performing parametric studies owing to its computational complexity)
- Flow is incompressible, even though the temperature changes. The temperature affects the flow only through buoyancy, causing upward momentum.

Domain: The physical domain set up for the problem is shown in Figure 2. The dashed lines define the boundaries of the city, which is modeled as a few building blocks with varying heights and widths. The temperature of the entire domain, except at the source, is kept at 300 K. At the source, a pollutant with mass diffusivity equal to 2.239E-5 m^2/s in air, and a temperature of 375 K is defined, to replicate toxic gas/aerosol emission and waste heat from the exhaust stack of a coal power plant.
The boundary conditions are set based on laminar flow assumptions. The ground is set as a no-slip wall, where neither x nor y-direction velocity is allowed. It is worth noting that the top boundary is set as a free-slip wall, allowing lateral motion of the flow, but disallowing penetration. This boundary condition replicates the effects of the uniform wind velocity continuing beyond the upper bound of our domain, as is physically the case. Without this boundary condition, misleading results of air flow exiting, and entering the domain in large amounts through the top bound are to be expected.

Boundary Conditions:

- Inlet: $u(0,y) = 2\ m/s;\ v(0,y) = 0;\ \partial P/\partial x\ (0,y)\ = 0;\ \partial T/\partial x\ (0,y)\ = 0;\ \partial \Phi/\partial x\ (0,y)\ = 0.$
- Outlet: $\partial u/\partial x\ (L,y) = 0, \partial v/\partial x\ (L,y) = 0, \partial P/\partial x\ (L,y)\ = 0;\ \partial T/\partial x\ (L,y)\ = 0;\ \partial \Phi/\partial x\ (L,y)\ = 0.$
- Ground: $u(x,0) = 0;\ v(x,0) = 0, \partial P/\partial y\ (x,0)\ = 0;\ \partial T/\partial y\ (x,0)\ = 0;\ \partial \Phi/\partial y\ (x,0)\ = 0$
- Top: $\partial u/\partial y(x,h) = 0;\ v(x,h) = 0;\ \partial P/\partial y\ (x,h)\ = 0;\ \partial T/\partial y\ (x,h)\ = 0;\ \partial \Phi/\partial y\ (x,h)\ = 0$
- Building walls: $u = 0;\ v = 0;\ \partial P/\partial x\ = 0;\ \partial T/\partial x\ = 0;\ \partial \Phi/\partial x\ = 0$
- Building ceilings: $u = 0;\ v = 0;\ \partial P/\partial y\ = 0;\ \partial T/\partial y = 0;\ \partial \Phi/\partial y = 0$

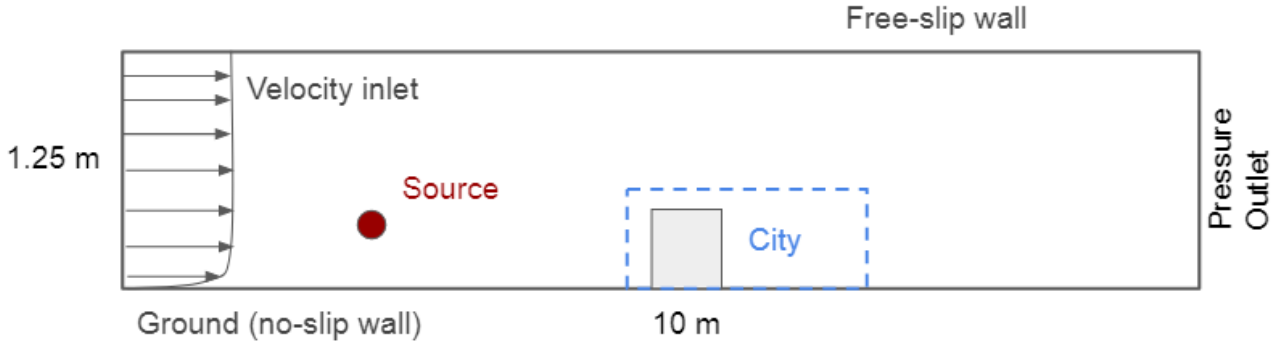

Figure 2: The physical domain in which discretized Navier-Stokes equations are solved

METHOD

Governing Equations: The following is a list of the governing equations of the problem. The momentum equations and the continuity equation serve to solve velocity and pressure fields, and the general transport equation is needed when solving the distribution of pollutant. In addition to the advective, diffusive and pressure terms, the y-momentum equation has an additional term of Boussinesq approximation, to approximate the buoyancy effect due to temperature. The reference temperature, T_{ref}, is set to 300 K, and the temperature, T, is acquired by solving the energy equation.

x-momentum: $\frac{\partial u}{\partial t} + \frac{\partial (uu)}{\partial x} + \frac{\partial (uv)}{\partial y} = -\frac{1}{\rho}\frac{\partial P}{\partial x} + \nu\left(\frac{\partial^2 u}{\partial x^2} + \frac{\partial^2 u}{\partial y^2}\right)$ (1)

y-momentum: $\frac{\partial v}{\partial t} + \frac{\partial (vu)}{\partial x} + \frac{\partial (vv)}{\partial y} = -\frac{1}{\rho}\frac{\partial P}{\partial y} + \nu\left(\frac{\partial^2 v}{\partial x^2} + \frac{\partial^2 v}{\partial y^2}\right) + \rho g \beta (T - T_{ref})$ (2)

Mass conservation: $\frac{\partial u}{\partial x} + \frac{\partial v}{\partial y} = 0$ (3)

Energy Equation: $\frac{\partial T}{\partial t} + \frac{\partial (uT)}{\partial x} + \frac{\partial (vT)}{\partial y} = \alpha_T\left(\frac{\partial^2 T}{\partial x^2} + \frac{\partial^2 T}{\partial y^2}\right) + Source_T$ (4)

General Transport: $\frac{\partial \phi}{\partial t} + \frac{\partial (u\phi)}{\partial x} + \frac{\partial (v\phi)}{\partial y} = \alpha_\phi\left(\frac{\partial^2 \phi}{\partial x^2} + \frac{\partial^2 \phi}{\partial y^2}\right) + Source_\phi$ (5)

Grid: To solve the above equations on a domain, it first has to be discretized. To do so the domain was discretized into a grid using a staggered grid approach. In this approach the pressure, u-velocity and v-velocity grid points are offset from each other. This approach ensures that a checkerboard pattern is not formed, which occurs in a collocated grid arrangement, where the variables are stored in the same position. This approach also replicates a control volume approach used in finite volume methods. To keep the matrices the same size, to avoid indexing difficulties, two columns of dummy nodes are added to *u*, and two rows of dummy nodes are attached to *v*, while pressure is solved on the interior of the cell, two dummy rows and columns were added, essentially padding the grid, these dummy nodes act as ghost nodes. To ensure consistency, we have stored the variables in a collocated manner.

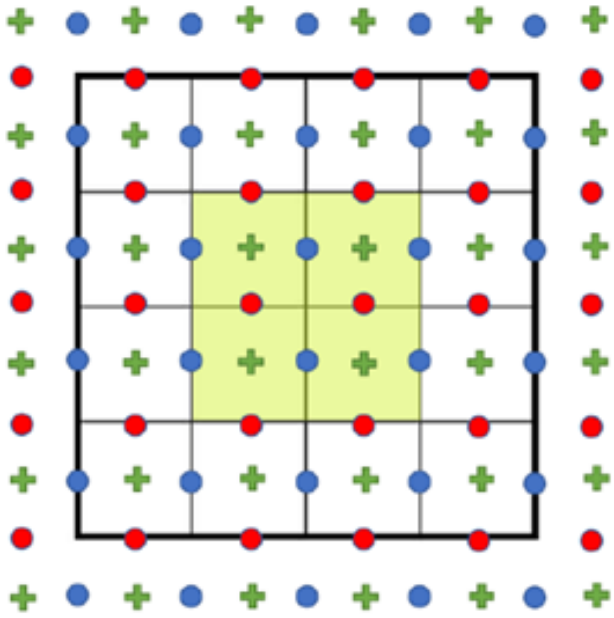

Figure 3. A section of the staggered grid: $u_{ij}$is to the right of P_{ij}, and $v_{ij}$is above P_{ij}. T_{ij} and $\Phi_{ij}$are stored at the same point as P_{ij}.

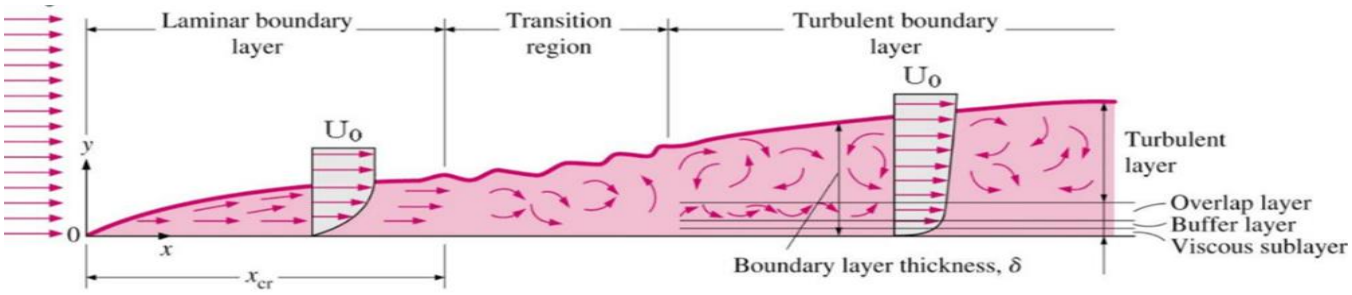

Figure 4. Boundary layer

Before we evaluate the solution on a uniform grid, we need to consider the need for a non-uniform grid. As our problem can be reduced to that of a fluid flow over a flat plate. In order to resolve the near wall effects due to the boundary layer flow, where the viscous effects of the fluid are significant. This is due to the no-slip condition on the wall. To evaluate the near wall effects, a very fine mesh is needed, this ensures that the boundary layer is accurately resolved. But refining the grid on the entire domain can be computationally cumbersome as the high discretization is not required where the flow is not chaotic or turbulent. So, as a trade-off, the grid is varied in the y direction. To accurately resolve the boundary layer, it is necessary to resolve the velocity profile near the wall [7,8]. A non-dimensional wall (y plus) distance is defined that bounds the near wall flow. It is defined as follows:

$y^+ \equiv \frac{u_*(\Delta y_0)}{\nu}$: (y plus) Dimensionless wall distance (6)

$u \equiv \sqrt{\frac{\tau_\omega}{\rho}}$: Friction velocity (7)

$\tau_\omega = \mu(\frac{\partial u}{\partial y})_{y=0}$: Wall shear stress (8)

The increase in grid is constant and follows a geometric progression. The progression is defined by the first layer height, the total number of grid points (as we want to restrict the total number of cells in our calculations) and the total height. Using the formula for the sum of a geometric progression, we can find the expansion ratio which governs the discretization in the y direction.

ϵ: Expansion ratio. $\epsilon = \frac{\Delta y_{i+1}}{\Delta y_i}$ (9)

Δy_0 : First layer height

y_{max}: Total height

N_y : Number of nodes in the y-direction

$\Delta y_0 \epsilon^{N_y} - y_{max}\epsilon + (y_{max} + \Delta y_0) = 0$ (10)

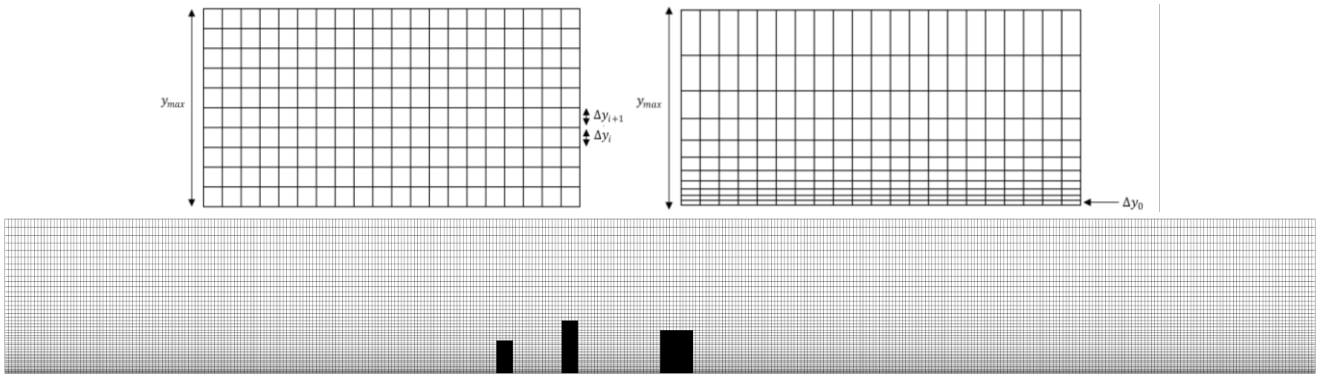

Figure 5. a) Uniform mesh b) Non-Uniform with expansion ratio c) The mesh grid generated for the simulation. The grid near the ground is inflated to capture the boundary layer of the flow. The rectangles represent buildings.

Using this discretization, we were able to achieve a wall $y^+ \approx 1$.

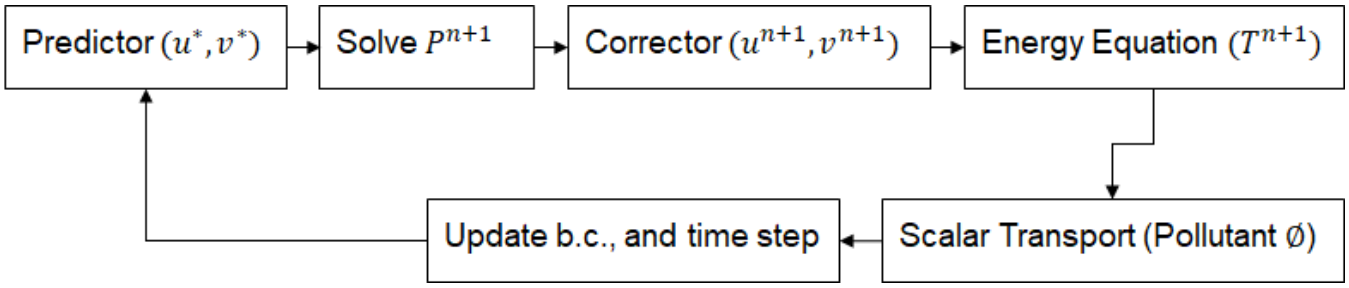

Figure 6. Flow of control for the Fractional Step Method

Fractional Step Method (FSM):
The workflow of the algorithm involves: 1. Initializing u, v, P and T matrices, 2. Defining boundary conditions, and 3. Time looping. The flow of time looping is shown in figure 6. The momentum equations and the mass conservation equation are solved, in steps 1 to 3, using the FSM method [9]. In step 6, a new time step size is calculated adaptively for the next time loop, to ensure the satisfaction of the Courant condition, namely,

$$\frac{|V|_{max}\Delta t}{\Delta x} \leq C_{max}, \qquad (11)$$

where $C_{max} = 0.65$, and thereby the stability of the code.

The output at each time step is shown next to the step names. Additionally, the energy and scalar transport equations can be solved simultaneously. The following are a list of the temporal discretization of coupled continuity and momentum equations used in FSM, in steps 1 to 3. where, $u^*$and v^* mark the intermediate velocity.

1. Predictor Step:

$$\frac{u^*-u^{(n)}}{\Delta t} = -\left(u\frac{\partial u}{\partial x} + v\frac{\partial u}{\partial y}\right)^{(n)} + \nu\left(\frac{\partial^2 u}{\partial x^2} + \frac{\partial^2 u}{\partial y^2}\right)^{(n)} \qquad (12)$$

$$\frac{v^*-v^{(n)}}{\Delta t} = -\left(u\frac{\partial v}{\partial x} + v\frac{\partial v}{\partial y}\right)^{(n)} + \nu\left(\frac{\partial^2 v}{\partial x^2} + \frac{\partial^2 v}{\partial y^2}\right)^{(n)} + \rho g\beta(T - T_{ref}) \qquad (13)$$

2. Pressure Poisson: $\left(\frac{\partial^2 P}{\partial x^2} + \frac{\partial^2 P}{\partial y^2}\right)^{(n+1)} = \frac{\rho}{\Delta t}\left(\frac{\partial u^*}{\partial x} + \frac{\partial v^*}{\partial y}\right)$ (14)

3. Corrector Step: $\frac{u^{(n+1)}-u^*}{\Delta t} = -\frac{1}{\rho}\frac{\partial P}{\partial x}$, $\frac{v^{(n+1)}-v^*}{\Delta t} = -\frac{1}{\rho}\frac{\partial P}{\partial y}$ (15)

Discretized Equations:
As shown in Figure 5b, the grid spacing changes along the y-direction, near the boundary layer. This had to be taken into account when discretizing the governing equations. $\Delta x_{ij}$and $\Delta y_{ij}$are used to reference the grid spacing to the right and above the spatial grid point (i, j). Ratios r_x and r_y are defined, and used in discretizing first and second-order spatial derivatives.

$$r_x = \frac{\Delta x_{ij}-\Delta x_{i-1,j}}{\Delta x_{ij}+\Delta x_{i-1,j}}, r_y = \frac{\Delta y_{ij}-\Delta y_{i,j-1}}{\Delta y_{ij}+\Delta y_{i,j-1}} \qquad (16,17)$$

1. Predictor Step:

$$u_{ij}^* = u_{ij}^{(n)} + \Delta t\left[Diff_{u_{ij}} - Adv_{u_{ij}}\right] \qquad (18)$$

$$v_{ij}^* = v_{ij}^{(n)} + \Delta t\left[Diff_{v_{ij}} - Adv_{v_{ij}}\right] + \rho g\beta\left(\frac{T_{ij}^{(n)}+T_{i,j+1}^{(n)}}{2} - T_{ref}\right) \qquad (19)$$

Where,

$$Diff_{u_{ij}} = \nu\left\{\frac{2\left[(1+r_x)u_{i-1,j}^{(n)} - 2u_{ij}^{(n)} + (1-r_x)u_{i+1,j}^{(n)}\right]}{\Delta x_{i-1,j}^2 + \Delta x_{ij}^2} + \frac{2\left[(1+r_y)u_{i,j-1}^{(n)} - 2u_{ij}^{(n)} + (1-r_y)u_{i,j+1}^{(n)}\right]}{\Delta y_{i,j-1}^2 + \Delta y_{ij}^2}\right\} \qquad (20)$$

$$Diff_{v_{ij}} = \nu\left\{\frac{2\left[(1+r_x)v_{i-1,j}^{(n)}-2v_{ij}^{(n)}+(1-r_x)v_{i+1,j}^{(n)}\right]}{\Delta x_{i-1,j}^2+\Delta x_{ij}^2}+\frac{2\left[(1+r_y)v_{i,j-1}^{(n)}-2v_{ij}^{(n)}+(1-r_y)v_{i,j+1}^{(n)}\right]}{\Delta y_{i,j-1}^2+\Delta y_{ij}^2}\right\} \quad (21)$$

$$Adv_{u_{ij}} = \frac{u_{ij}^{(n)}\left(u_{i+1,j}^{(n)}-u_{i-1,j}^{(n)}\right)}{\Delta x_{i-1,j}+\Delta x_{i,j}}+\frac{v_{i-1,j}^{(n)}+v_{ij}^{(n)}+v_{i-1,j+1}^{(n)}+v_{i,j+1}^{(n)}}{4}\frac{u_{i,j+1}^{n}-u_{i,j-1}^{(n)}}{\Delta y_{i,j-1}+\Delta y_{ij}} \quad (22)$$

$$Adv_{v_{ij}} = \frac{v_{ij}^{(n)}\left(v_{i,j+1}^{(n)}-v_{i,j-1}^{(n)}\right)}{\Delta y_{i,j-1}+\Delta y_{ij}}+\frac{u_{i,j-1}^{(n)}+u_{ij}^{(n)}+u_{i+1,j-1}^{(n)}+u_{i+1,j}^{(n)}}{4}\frac{v_{i+1,j}^{n}-v_{i-1,j}^{(n)}}{\Delta x_{i-1,j}+\Delta x_{ij}} \quad (23)$$

2. Pressure Poisson:

$$P_{ij}^{(n+1)} = \left(\frac{4}{\Delta x_{i-1,j}^2+\Delta x_{ij}^2}+\frac{4}{\Delta y_{i,j-1}^2+\Delta y_{ij}^2}\right)^{-1}\left\{\frac{2\left[(1-r_x)P_{i+1,j}^{(n)}+(1+r_x)P_{i-1,j}^{(n)}\right]}{\Delta x_{i-1,j}^2+\Delta x_{ij}^2}+\frac{2\left[(1-r_y)P_{i,j+1}^{(n)}+(1+r_y)P_{i,j-1}^{(n)}\right]}{\Delta y_{i,j-1}^2+\Delta y_{ij}^2}-\frac{\rho}{\Delta t}\left[\frac{u_{i+1,j}^{*}-u_{i-1,j}^{*}}{\Delta x_{ij}+\Delta x_{i-1,j}}+\frac{v_{i,j+1}^{*}-v_{i,j-1}^{*}}{\Delta y_{ij}+\Delta y_{i,j-1}}\right]\right\} \quad (24)$$

3. Corrector: $u_{ij}^{(n+1)} = u_{ij}^{(n)} - \frac{\Delta t}{\rho}\frac{P_{i+1,j}^{(n+1)}-P_{ij}^{(n+1)}}{\Delta x_{ij}}$; $v_{ij}^{(n+1)} = v_{ij}^{(n)} - \frac{\Delta t}{\rho}\frac{P_{i,j+1}^{(n+1)}-P_{ij}^{(n+1)}}{\Delta y_{ij}}$ (25,26)

4. Energy Equation: (using first order upwinding method)

$$U = \frac{u_{ij}+u_{i-1,j}}{2},\ V = \frac{v_{ij}+v_{i,j-1}}{2} \quad (27,28)$$

$\boldsymbol{U>0}$, $\boldsymbol{V>0}$

$$T_{ij}^{(n+1)} = T_{ij}^{(n)} + \Delta t\left\{2\alpha_T\left(\frac{(1-r_x)T_{i+1,j}-2T_{ij}+(1+r_x)T_{i-1,j}}{\Delta x_{i-1,j}^2+\Delta x_{ij}^2}+\frac{(1-r_y)T_{i,j+1}-2T_{ij}+(1+r_y)T_{i,j-1}}{\Delta y_{i,j-1}^2+\Delta y_{ij}^2}+S_T\right)-\left(U\left(\frac{T_{i,j}+T_{i-1j}}{\Delta x_{i-1,j}}\right)+V\left(\frac{T_{ij}+T_{i,j-1}}{\Delta y_{i,j-1}}\right)\right)\right\} \quad (29)$$

$\boldsymbol{U<0}$, $\boldsymbol{V>0}$

$$T_{ij}^{(n+1)} = T_{ij}^{(n)} + \Delta t\left\{2\alpha_T\left(\frac{(1-r_x)T_{i+1,j}-2T_{ij}+(1+r_x)T_{i-1,j}}{\Delta x_{i-1,j}^2+\Delta x_{ij}^2}+\frac{(1-r_y)T_{i,j+1}-2T_{ij}+(1+r_y)T_{i,j-1}}{\Delta y_{i,j-1}^2+\Delta y_{ij}^2}+S_T\right)-\left(U\left(\frac{T_{i+1,j}+T_{ij}}{\Delta x_{i,j}}\right)+V\left(\frac{T_{ij}+T_{i,j-1}}{\Delta y_{i,j-1}}\right)\right)\right\} \quad (30)$$

$\boldsymbol{U>0}$, $\boldsymbol{V<0}$

$$T_{ij}^{(n+1)} = T_{ij}^{(n)} + \Delta t\left\{2\alpha_T\left(\frac{(1-r_x)T_{i+1,j}-2T_{ij}+(1+r_x)T_{i-1,j}}{\Delta x_{i-1,j}^2+\Delta x_{ij}^2}+\frac{(1-r_y)T_{i,j+1}-2T_{ij}+(1+r_y)T_{i,j-1}}{\Delta y_{i,j-1}^2+\Delta y_{ij}^2}+S_T\right)-\left(U\left(\frac{T_{i,j}+T_{i-1j}}{\Delta x_{i-1,j}}\right)+V\left(\frac{T_{ij+1}+T_{i,j}}{\Delta y_{i,j}}\right)\right)\right\} \quad (31)$$

$\boldsymbol{U<0}$, $\boldsymbol{V<0}$

$$T_{ij}^{(n+1)} = T_{ij}^{(n)} + \Delta t\left\{2\alpha_T\left(\frac{(1-r_x)T_{i+1,j}-2T_{ij}+(1+r_x)T_{i-1,j}}{\Delta x_{i-1,j}^2+\Delta x_{ij}^2}+\frac{(1-r_y)T_{i,j+1}-2T_{ij}+(1+r_y)T_{i,j-1}}{\Delta y_{i,j-1}^2+\Delta y_{ij}^2}+S_T\right)-\left(U\left(\frac{T_{i+1,j}+T_{ij}}{\Delta x_{i,j}}\right)+V\left(\frac{T_{ij+1}+T_{i,j}}{\Delta y_{i,j}}\right)\right)\right\} \quad (32)$$

5. General Transport Equations: (using first order upwinding method)

$$U = \frac{u_{ij}+u_{i-1,j}}{2},\ V = \frac{v_{ij}+v_{i,j-1}}{2} \quad (33,34)$$

$\boldsymbol{U>0}$, $\boldsymbol{V>0}$

$$\phi_{ij}^{(n+1)} = \phi_{ij}^{(n)} + \Delta t \left\{ 2\alpha_\phi \left(\frac{(1-r_x)\phi_{i+1,j} - 2\phi_{ij} + (1+r_x)\phi_{i-1,j}}{\Delta x_{i-1,j}^2 + \Delta x_{ij}^2} + \frac{(1-r_y)\phi_{i,j+1} - 2\phi_{ij} + (1+r_y)\phi_{i,j-1}}{\Delta y_{i,j-1}^2 + \Delta y_{ij}^2} + S_\phi \right) - \left(U \left(\frac{\phi_{i,j} + \phi_{i-1j}}{\Delta x_{i-1,j}} \right) + V \left(\frac{\phi_{ij} + \phi_{i,j-1}}{\Delta y_{i,j-1}} \right) \right) \right\} \quad (35)$$

$\boldsymbol{U < 0}$, $\boldsymbol{V > 0}$

$$\phi_{ij}^{(n+1)} = \phi_{ij}^{(n)} + \Delta t \left\{ 2\alpha_\phi \left(\frac{(1-r_x)\phi_{i+1,j} - 2\phi_{ij} + (1+r_x)\phi_{i-1,j}}{\Delta x_{i-1,j}^2 + \Delta x_{ij}^2} + \frac{(1-r_y)\phi_{i,j+1} - 2\phi_{ij} + (1+r_y)\phi_{i,j-1}}{\Delta y_{i,j-1}^2 + \Delta y_{ij}^2} + S_\phi \right) - \left(U \left(\frac{\phi_{i+1,j} + \phi_{ij}}{\Delta x_{i,j}} \right) + V \left(\frac{\phi_{ij} + \phi_{i,j-1}}{\Delta y_{i,j-1}} \right) \right) \right\} \quad (36)$$

$\boldsymbol{U > 0}$, $\boldsymbol{V < 0}$

$$\phi_{ij}^{(n+1)} = \phi_{ij}^{(n)} + \Delta t \left\{ 2\alpha_\phi \left(\frac{(1-r_x)\phi_{i+1,j} - 2\phi_{ij} + (1+r_x)\phi_{i-1,j}}{\Delta x_{i-1,j}^2 + \Delta x_{ij}^2} + \frac{(1-r_y)\phi_{i,j+1} - 2\phi_{ij} + (1+r_y)\phi_{i,j-1}}{\Delta y_{i,j-1}^2 + \Delta y_{ij}^2} + S_\phi \right) - \left(U \left(\frac{\phi_{i,j} + \phi_{i-1j}}{\Delta x_{i-1,j}} \right) + V \left(\frac{\phi_{ij+1} + \phi_{i,j}}{\Delta y_{i,j}} \right) \right) \right\} \quad (37)$$

$\boldsymbol{U < 0}$, $\boldsymbol{V < 0}$

$$\phi_{ij}^{(n+1)} = \phi_{ij}^{(n)} + \Delta t \left\{ 2\alpha_\phi \left(\frac{(1-r_x)\phi_{i+1,j} - 2\phi_{ij} + (1+r_x)\phi_{i-1,j}}{\Delta x_{i-1,j}^2 + \Delta x_{ij}^2} + \frac{(1-r_y)\phi_{i,j+1} - 2\phi_{ij} + (1+r_y)\phi_{i,j-1}}{\Delta y_{i,j-1}^2 + \Delta y_{ij}^2} + S_\phi \right) - \left(U \left(\frac{\phi_{i+1,j} + \phi_{ij}}{\Delta x_{i,j}} \right) + V \left(\frac{\phi_{ij+1} + \phi_{i,j}}{\Delta y_{i,j}} \right) \right) \right\} \quad (38)$$

DISCUSSION OF RESULTS

Snapshots of the velocity and pressure results are shown in Figures 7-11. Overall, uniform flow can be seen in the first quarter of the domain, before the flow encounters the buildings. The growth of the boundary layer can also be observed in Figures 7, 9 and 10, as the low speed (deep blue) layer near ground thickens moving from left to right. The flow passing over the city gets accelerated, as shown as the darkening of the redness in the speed contour and streamline plots.

Stagnation of pressure is seen in front of the first building (Figure 11), which was expected. The high-speed flow over the city causes the pressure over the city to drop, compared to the region upstream of the city. Inside the city, between the buildings, a low-pressure region is observed due to a lack of fluid flow in that region. In the wake of the city, vortex shedding due to flow separation can be observed in figures 10 and 11. In the same domain locations, in the pressure contour plot, low pressure regions are found, which correspond to the vortices.

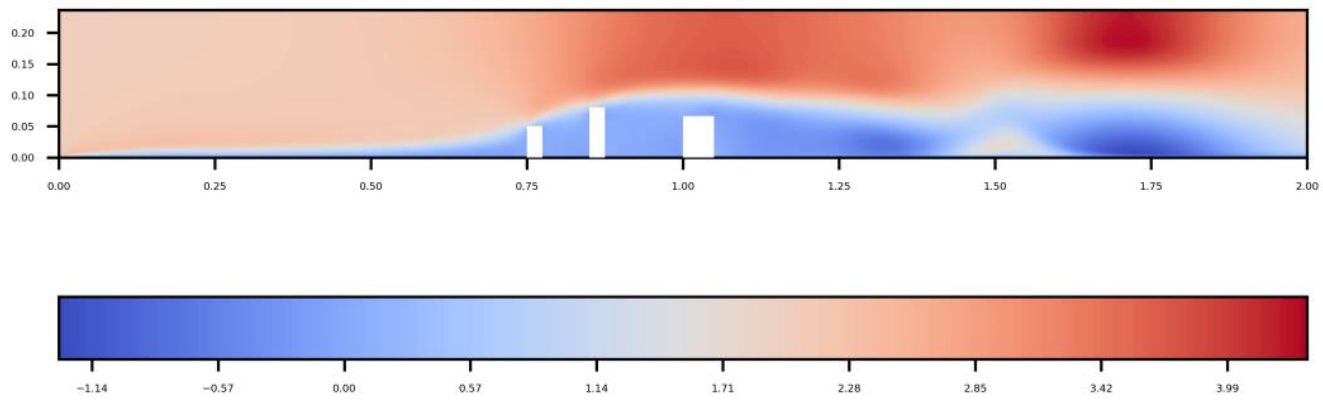

Figure 7. The contour plot of x-velocity at the end time.

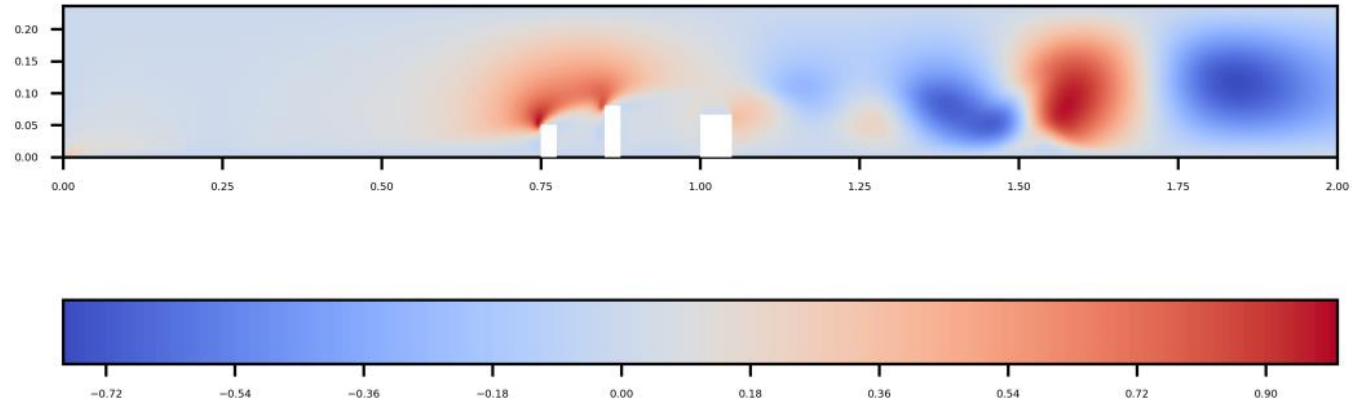

Figure 8. The contour plot of y-velocity at the end time.

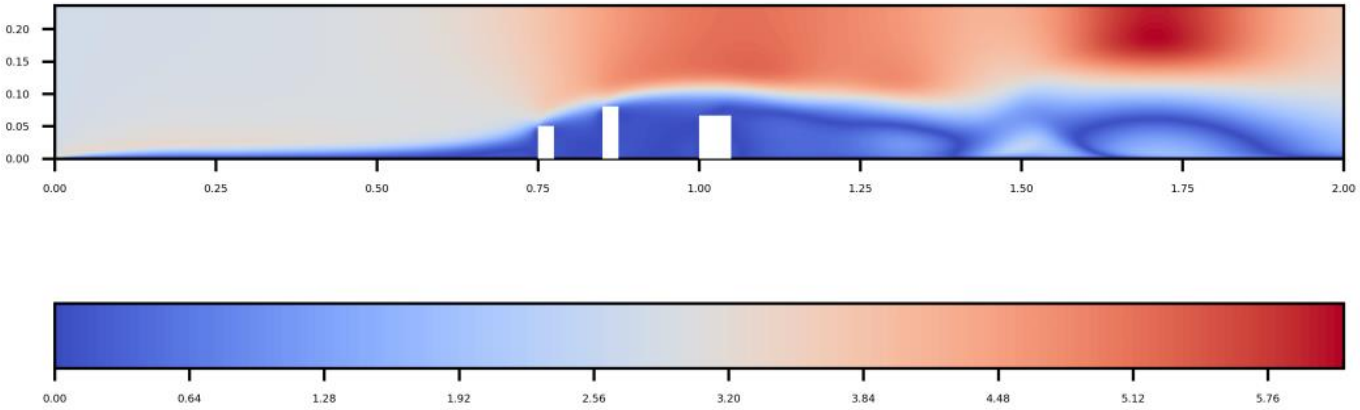

Figure 9. The contour plot of the magnitude of velocity at the end time.

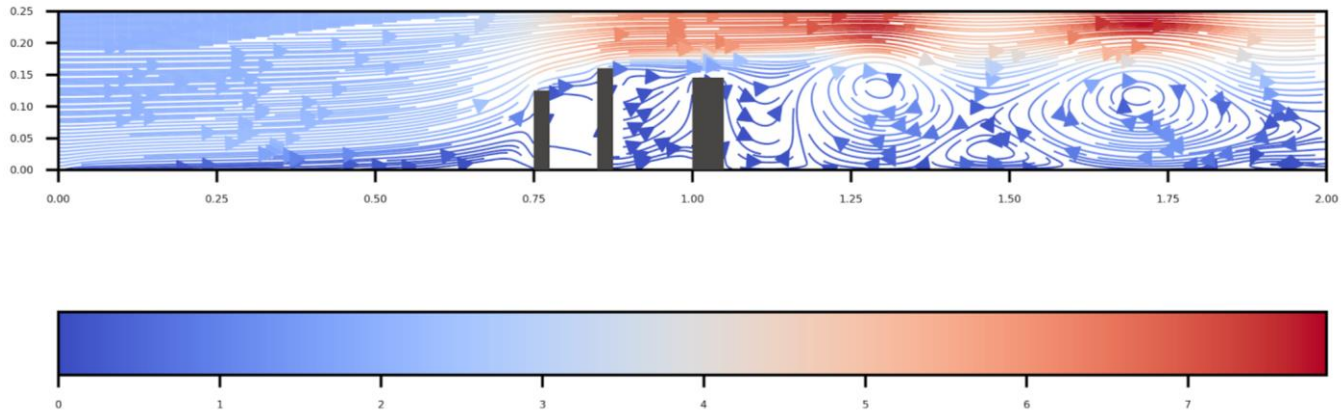

Figure 10. The streamline plot of the flow at the end time.

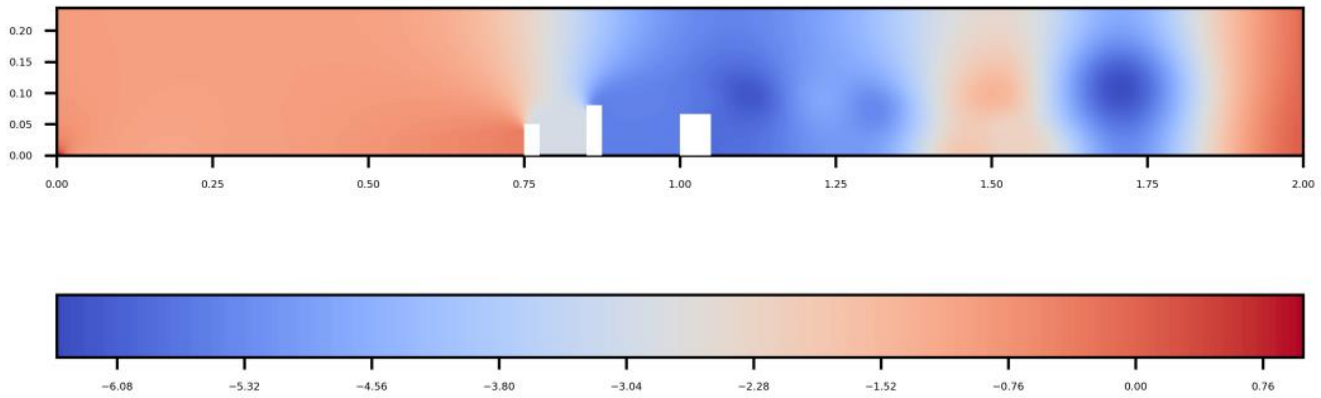

Figure 11. The contour plot of the relative pressure at the end time.

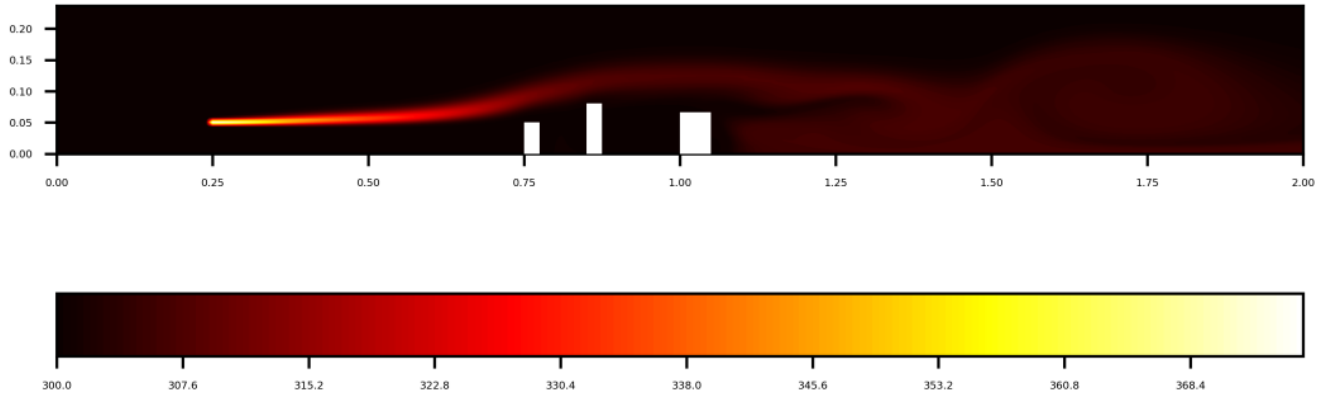

Figure 12. The contour plot of temperature at the end time

A snapshot of the temperature contour is shown in figure 12. A temperature source was introduced with a constant temperature of 375 K ($\approx 100^{o}C$), which was chosen to represent the temperature of a coal-fired power plant stack. The temperature is transported by the wind towards the city, leading to a rise in ambient temperature around the city. Also, since we are coupling energy equation to the momentum equation using the Boussinesq term, the transport of temperature produces buoyancy effects.

The average rise in temperature for the three different locations of sources has been shown in figure 13. The highest rise in ambient temperatures within the city is seen in the lower source with lesser values seen for higher source. For the central source, the average temperature rise lies in between the lower and higher values.

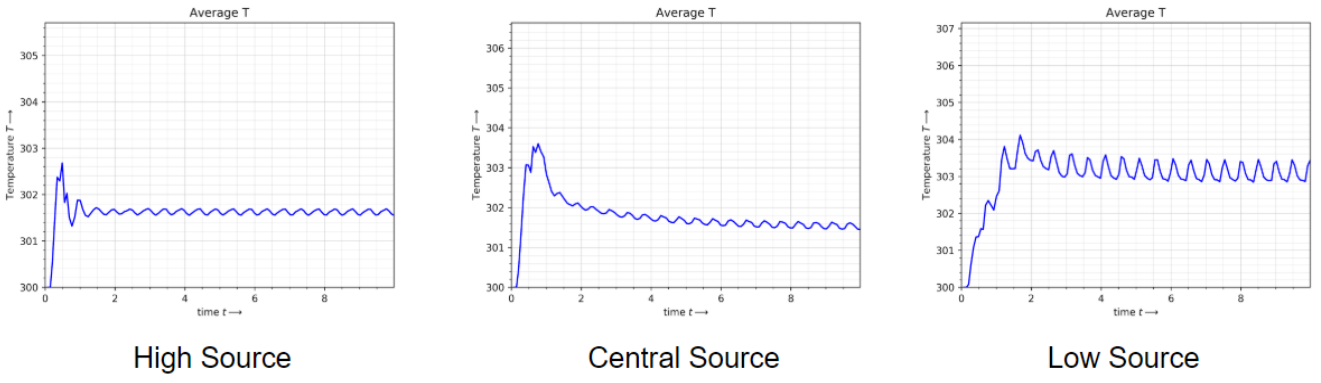

Figure 13: Average temperature inside the city given three different source locations.

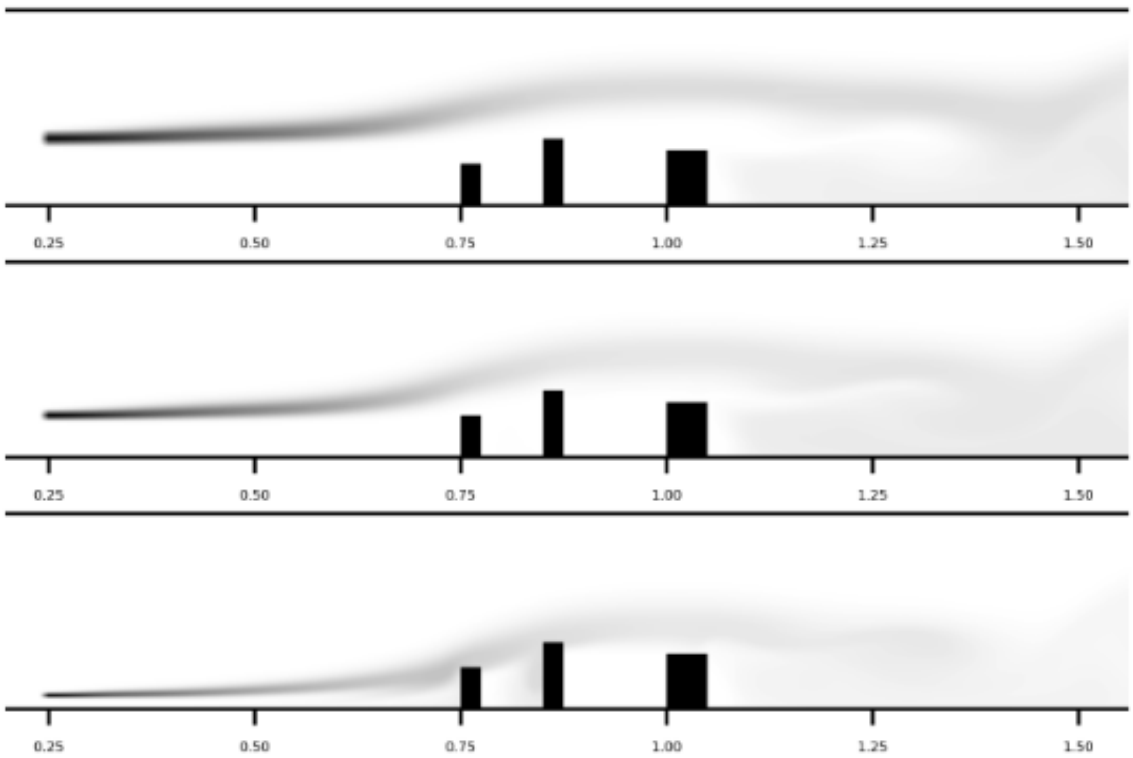

Figure 14. Pollutant distribution with source at different heights.

The contour plots of the pollutant concentration are shown in Figure 14, with varying source height. The three sub-plots show the distribution of the pollutant at the same time step. While buildings can shield the inhabitants from pollutants, they also create vortices such that pollutants get sucked into the space behind buildings. This is what is seen in the lower and central sources. With a high source, the pollutant carried in the flow easily passes over the buildings without much interaction with the region inside the city. As the source is lowered, the city buildings interfere with the pollutant more, until as shown in the bottom plot of figure 14, the pollutant gets temporarily trapped between the first two buildings.

Although the bulk of the pollutants that enter the space between the buildings eventually leaves and gets carried downwind, some remnants are always left behind. It especially doesn't help if the building heights increase in sequence, where the taller building downstream makes it difficult for the trapped pollutant to leave. If, however, the first building is taller than the subsequent one, then the flow can get out more easily when trapped. Thus, when building a power plant upwind of a city, it should not be along the path of dominant trade winds.

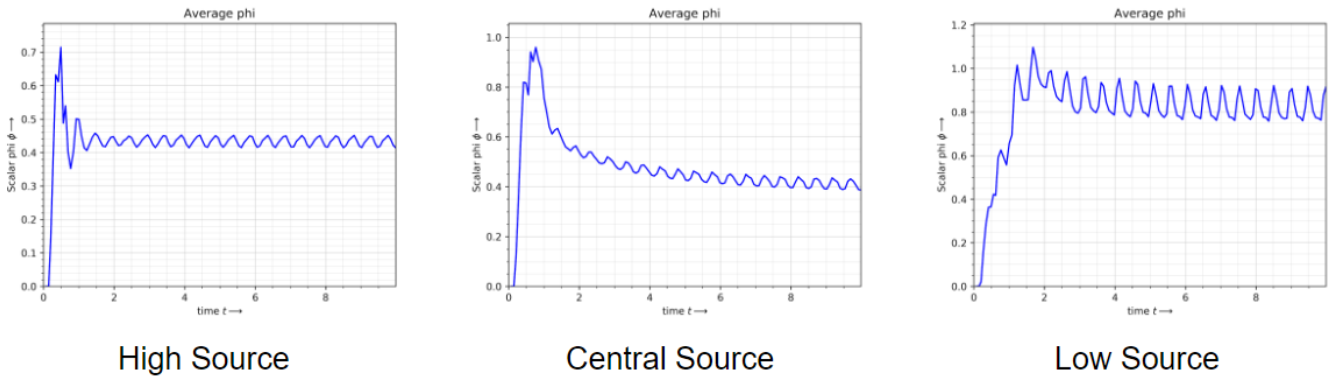

Figure 15: Concentration of the pollutant in the city as a function of time.

	Low	Central	High
Uniform	0.780362	0.411214	0.45042
Ascending	1.217034	0.620012	0.548575
Descending	0.735992	0.362999	0.376689

Table 1: Average pollutant concentration for different configurations of buildings (uniform, ascending and descending) and sources (low, high and central).

PARAMETRIC STUDY:

In order to better understand the effects of building dimensions and location of source on the accumulation of pollutants, a parametric study was carried out. Three different building configurations (uniform, ascending and descending) were considered, along with three different locations for the pollutant source (low, high and central). The average concentration of the pollutants was calculated within the city for every permutation of building configuration and height of pollutant source. The pollutant is initialized upstream of the buildings with a value of 20 units. The concentration was averaged over the time period of 4 -10 seconds. The results of the study have been tabulated in Table 1.

From Table 1 and Fig 16, 17 and 18, it is evident that the building configuration as well as the source location affect the pollutant concentration within the city greatly. A low source results in high pollutant concentrations since most of the pollutants are trapped in between the buildings. Also, the ascending building configuration traps a large amount of pollutant as compared to the other configurations.

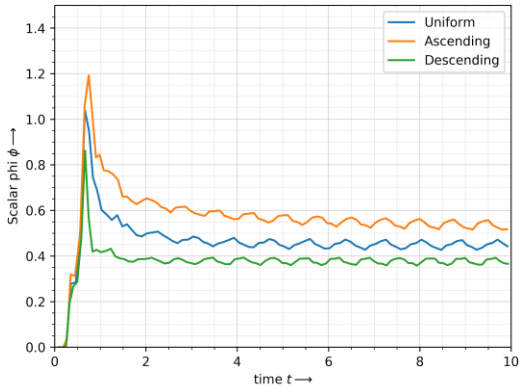

Figure 16: Concentration of Pollutant for High Source

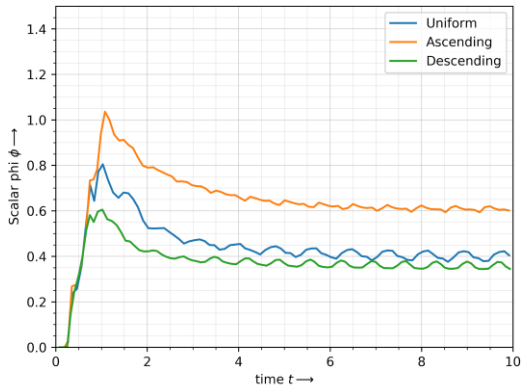

Figure 17: Concentration of Pollutant for Central Source

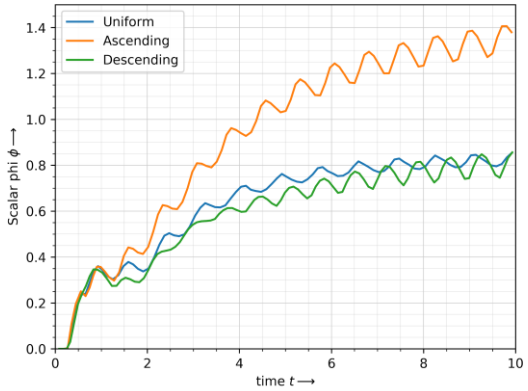

Figure 18: Concentration of Pollutant for Low Source

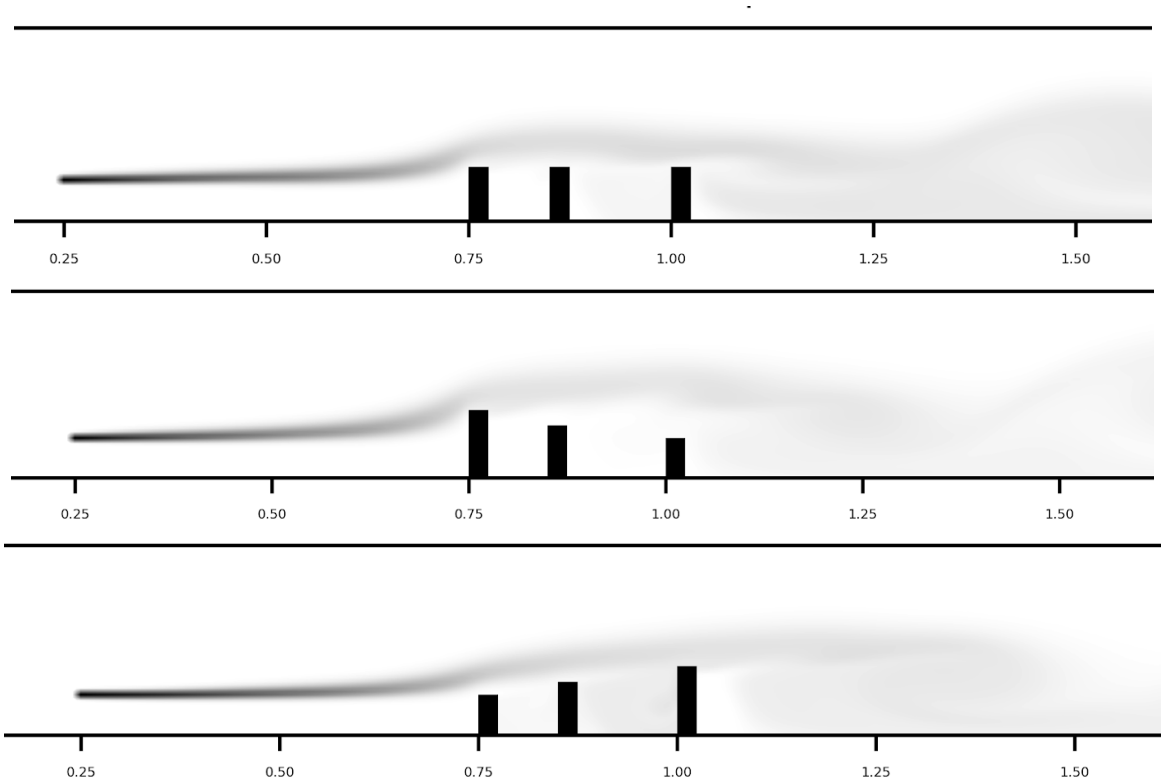

Figure 19: Pollutant distribution for different building configurations for a central source

An interesting observation about the plots is that the average concentrations keep fluctuating. This can be explained by the vortex shedding that can be seen in the wake of the buildings, due to which steady state is not attained. Additionally, in the plot for a low source [Fig 18], the average concentration doesn't converge but rather keeps on increasing. This is because in this case, most of the pollutant gets trapped between the buildings especially in the ascending building configuration with a low source.

Large Eddy Simulation:

In most atmospheric modelling simulations, turbulence is a key consideration [6], as flows are of that nature due to the high Reynolds number. To adapt our model to simulate turbulence we followed the Smagorinsky-Lilly model for estimating the turbulent viscosity. The addition of a turbulent viscosity term essentially means that we are carrying out a large eddy simulation.

In the Smagorinsky-Lilly model, the eddy viscosity is modeled by $\mu_{sgs} = \rho(C_s\Delta)^2|\underline{S}|$ (39)

where the filter width is usually taken to be: $\Delta = (\text{Volume})^{1/3}$ (40)

and $\underline{S} = \sqrt{2S_{ij}S_{ij}}$, with $S_{ij} = \frac{1}{2}(\frac{\partial \underline{u}}{\partial y} + \frac{\partial \underline{v}}{\partial x})$. (41)

The effective viscosity is calculated from: $\mu_{eff} = \mu_{mol} + \mu_{sgs}$ (42)

The Smagorinsky constant is usually taken to be $C_s = 0.2$.

The CFD simulation was successfully carried out using the LES solver. However, owing to the computational complexity, parametric studies were not performed using the LES solver.

CONCLUSION

The atmospheric flow around a city successfully modelled using a Navier-Stokes LES solver. Additionally, the transport of Temperature and Pollutants was parametrically studied using a laminar model.

It was observed that the close vicinity to polluting sources can gravely affect the air quality of a city due to accumulation of pollutants and the rise in average temperatures.
Furthermore, it was observed that the pollutant and temperature distributions were highly sensitive to building configuration (height, dimension and spacing), wind velocity and source location.
Finally, it was concluded that the computational modelling of pollutant flow can be a useful tool in setting up of regulations regarding the city layout as well as the location of power plants with respect to cities.

REFERENCES:

[1] Vox, "The Fight to Rethink (and Reinvent) Nuclear Power." *YouTube*, commentary by M. Sajanya, May 17, 2017, https://www.youtube.com/watch?v=poPLSgbSO6k
[2] Alice Lippert, Office of Electricity Delivery & Energy Reliability, U.S. Department of Energy "State of Pennsylvania Energy Sector Risk Profile." Retrieved in 12/2019 from https://www.energy.gov/sites/prod/files/2015/05/f22/PA-Energy%20Sector%20Risk%20Profile.pdf
[3] U.S. Department of Energy, Energy Information Administration, Independent Statistics and Analysis, *Pennsylvania State Profile and Analysis*. Retrieved in 12/2019 from https://www.eia.gov/state/?sid=PA#tabs-4
[4] Von Kármán, Th. (1930), "Mechanische Ähnlichkeit und Turbulenz", *Nachrichten von der Gesellschaft der Wissenschaften zu Göttingen, Fachgruppe 1 (Mathematik)*, **5**: 58–76 (also as: "Mechanical Similitude and Turbulence", Tech. Mem. NACA, no. 611, 1931).
[5] Mohrig, David (2004). "Conservation of Mass and Momentum" (PDF). *12.110: Sedimentary Geology, Fall 2004*. MIT OCW. Retrieved 2009-03-27.
[6] Turbulent Flows (2000) pp. 273–274.Pope, Stephen (2000), *Turbulent Flows* (1st revised ed.), Cambridge University Press, ISBN 0-521-59125-2
[7] https://www.simscale.com/forum/t/what-is-y-yplus/82394
[8] Frank M. White's *Fluid Mechanics* 5th edition, page 467
[9] http://www.montana.edu/mowkes/research/source-codes/GuideToCFD.pdf